SSRG International Journal of Geo-informatics and Geological Science
ISSN: 2393–9206 / https://doi.org/10.14445/23939206/IJGGS-V11I2P101

Volume 11 Issue 2, 1-16, May-Aug 2024


*Original Article*

# Impact Analysis of Sanjay Gandhi Thermal Power Station (SGTPS) over the Surrounding Forest Using Remote Sensing and GIS Techniques

Surabhi Soni[1], Jyoti Sarup[2]

[1,2]*Department of Civil Engineering, Maulana Azad National Institute of Technology, Bhopal, Madhya Pradesh, India.*

[1]*Corresponding Author : surabhi.soni28@gmail.com*

Received: 25 April 2024 Revised: 02 June 2024 Accepted: 20 June 2024 Published: 08 July 2024

***Abstract*** *- Dependence on thermal power plants (TPPs) for massive power generation leads to many consequences, such as changes in temperature and increasing pollution levels, which adversely affect human and vegetation health. So, proper maintenance and monitoring of TPPs are crucial, but to accomplish this, the traditional in-situ inspections prove time-consuming, labour-intensive, and financially impractical. This research proposes the application of Remote Sensing (RS) and Geographical Information System (GIS) techniques as powerful tools to mitigate these challenges significantly. This study aims to analyze the impact of the SGTPS and its emitted pollutants on its surrounding forest confined within the two buffer zones by assessing the correlation between various indices (Soil Moisture Index (SMI), Land Surface Temperature (LST), Normalized Difference Vegetation Index (NDVI)), and pollutants ($SO_2$, $NO_x$, PM, CO) emitted and changes in forest cover through Land Use and Land Cover (LULC) change detection. The study also seeks to identify the reasons behind the observed variations. Consequently, it aims to offer insightful information that can support evidence-based decision-making and sustainable management techniques for the preservation of the irreplaceable forest ecosystems that border the SGTPS. Despite some observed variations, overall analysis suggests that the studied SGTPS has minimal impact on forest health, likely due to adherence to regulations and pollution mitigation efforts. Similar assessments nationwide could ensure sustainable energy production while meeting environmental standards.*

***Keywords*** *- GIS, LULC, NDVI, Remote sensing, SGTPS.*

## 1. Introduction

Forests are essential for the Earth's ecological balance, providing vital resources for human survival. However, escalating anthropogenic activities and pollution pose severe threats to flora and fauna. In the contemporary technology-driven era, power demand has led to a reliance on various energy resources, especially TPPs. In India, the Ministry of Coal reports that a predominant 75% of electricity production is derived from coal-based thermal power plants, [1] making it a crucial component of the nation's power generation. However, the emissions from these power stations pose significant threats to both human health and natural ecosystems, particularly forests. The pollutants released cause air pollution, acid rain, [2,3] leaf stomata clogging [4,5], which adversely impact plant chlorophyll content and result in damage of vegetation as well as narrowing of annual tree growth rings, leading to substandard timber and economic losses. [6]

While these plants significantly contribute to power generation, their proper maintenance and monitoring are crucial. Traditional in-situ methods of Environment Impact Analysis (EIA) are time-consuming and costly, [7,8] prompting the exploration of efficient alternatives. In recent years, RS and GIS have emerged as indispensable tools for monitoring and analyzing such ecological changes.

RS involves acquiring information about a target without direct contact [9], while GIS is a system for inputting, organizing, analyzing, and mapping various data, particularly geographic data. Both RS and GIS exhibit significant potential in forest ecology management, ranging from species identification to monitoring forest health and estimating vegetation biomass. [10-13] Numerous studies have utilized different satellite data for classification and land use and land cover mapping, [14,15] change detection, [16] and pollution analysis. [17,18] Additionally, RS and GIS facilitate the estimation of crucial vegetation health indices such as the SMI, LST, and NDVI. [18-21]

Kantarci (2003) examined how three thermoelectric power plants affected the Yerkesik-Denizova woodlands in

Mugla Province, Turkey.[6] Environmental assessments were used to determine how these power installations affected forest health. Although the study offered valuable insights, it was limited by a lack of long-term data on pollution levels and their effects on biodiversity. In contrast, Mondal et al. (2016) simulated the environmental impacts of the West Bengal Kolaghat thermal power station using modern RS and GIS tools. The study attempted to identify land use and pollutant changes by analyzing satellite images and geographical data. The study struggled to detect small-scale environmental changes due to the low resolution of available satellite images. [22] Padmavathi et al. (2015) assessed air pollution around the Dr Narla Tata Rao Thermal Power Station (NTTPS). The examination of significant air contaminants was helpful, but its regional and temporal scope may have missed pollution dynamics trends. [23] Chowdhury (2017) examined how the Rampal coal-fired power plant affected the Sundarbans, the world's most extensive mangrove forest. The study used field observations, data analysis, and literature evaluation to clarify ecological issues. Secondary data and forecasts may have obscured direct environmental effects. [24] Yadav and Prakash (2014) examined the existing scenario and environmental impacts of thermal power facility emissions in India. Despite the beneficial insights from emission data synthesis and regulatory compliance analysis, data accuracy and the lack of reported emissions may have influenced the study's conclusions. [25] Using spatial information research, Kumari and Sarma (2017) investigated how land use surrounding a thermal power plant in the Singrauli area of Madhya Pradesh related to shifting patterns in land surface temperature. However, the study could benefit from a more extensive temporal analysis to better understand long-term trends. [26] These collaborative efforts highlight the complex nature of comprehending the environmental impacts of thermal power plant operations. Also, although many studies have looked at how TPPs impact vegetation and forests in general, [6] [22-26] there is still a significant gap in understanding how SGTPS affects its surrounding forest explicitly, using RS and GIS techniques.

The Sanjay Gandhi Thermal Power Station, located in lush green forests, serves as an exemplary case for studying industrial impacts on surrounding forest health. Unlike previous research that typically focuses on isolated aspects, this study comprehensively analyzes multiple factors, including LST, SMI, LULC changes, and pollutant levels on forest health, and examines the correlations between them using a simple yet innovative approach. Notably, it employs a comparative analysis between two buffer zones and examines data from two distinct years. Additionally, the study investigates potential reasons behind the observed changes and monitors whether various indices value, pollutant levels, and stack height comply with established standards. A significant novelty of this research lies in its simple yet effective methodology, and by zooming in on this specific area, the goal is to provide detailed insights that can help with conservation efforts tailored to the unique characteristics of the SGTPS surroundings, making it highly advantageous for conducting similar environmental impact studies.

## 2. Study Area

The study was conducted for the SGTPS situated at latitude 23°18′21″ N and longitude 81°03′54″ E, along with its surrounding area within two designated circular buffer zones. The first zone extended from a radial distance of 2.75 km, centered at the main stack of SGTPS, while the second spanned from 2.75 km to 5.5 km from SGTPS in Birsinghpur, Umaria district, Madhya Pradesh, India **(Figure 1)**. The selection of these buffer zones is based on the conclusion that the highest concentrations of sulfur dioxide ($SO_2$) and nitrogen dioxide ($NO_2$) occur within a 5 km radius, as reported by the Central Electricity Authority (CEA). [27]

## 3. Data and Methods

### *3.1. Derivation of River Network and Watershed Using Digital Elevation Model (DEM) for Region of Interest (ROI) and Buffer Zone Creation*

For the analysis, an appropriate administrative border was investigated through various toposheets of administrative borders at state, district and village levels obtained from the Survey of India (SOI) containing the ROI; however, it was not appropriately circumscribed within any such boundary.

By utilizing the standard watersheds provided by the Integrated Watershed Management Programme (IWMP), It has been identified that the area of interest is situated within watershed 2A6H4, which corresponds to the mainstream of the Johila River that flows through the study region. So, to derive the most recent watershed for the same region, Shuttle Radar Topography Mission-DEM (SRTM-DEM) data was downloaded for the ROI from the United States Geological Survey EarthExplorer (USGS EE) website. [28] It was found that two tiles contained the required ROI. So, after processing the DEM from the SRTM, these two tiles were mosaicked. Using this mosaicked DEM and Quantum Geographic Information System (QGIS) tools, a river network was derived. Out of this river network, the critical stream running through the study area was determined (Figure 2), which is further used to obtain its watershed, and its shape file is created as the study area boundary.

As the next step for analysis, buffer zones were created using QGIS software's Geoprocessing tools at a radial distance of 2.75 km and another one from 2.75 km to 5.5 km around the central stack of SGTPS to study its impact on the surrounding forest. Their respective shape files were also created for further analysis (Figure 3).

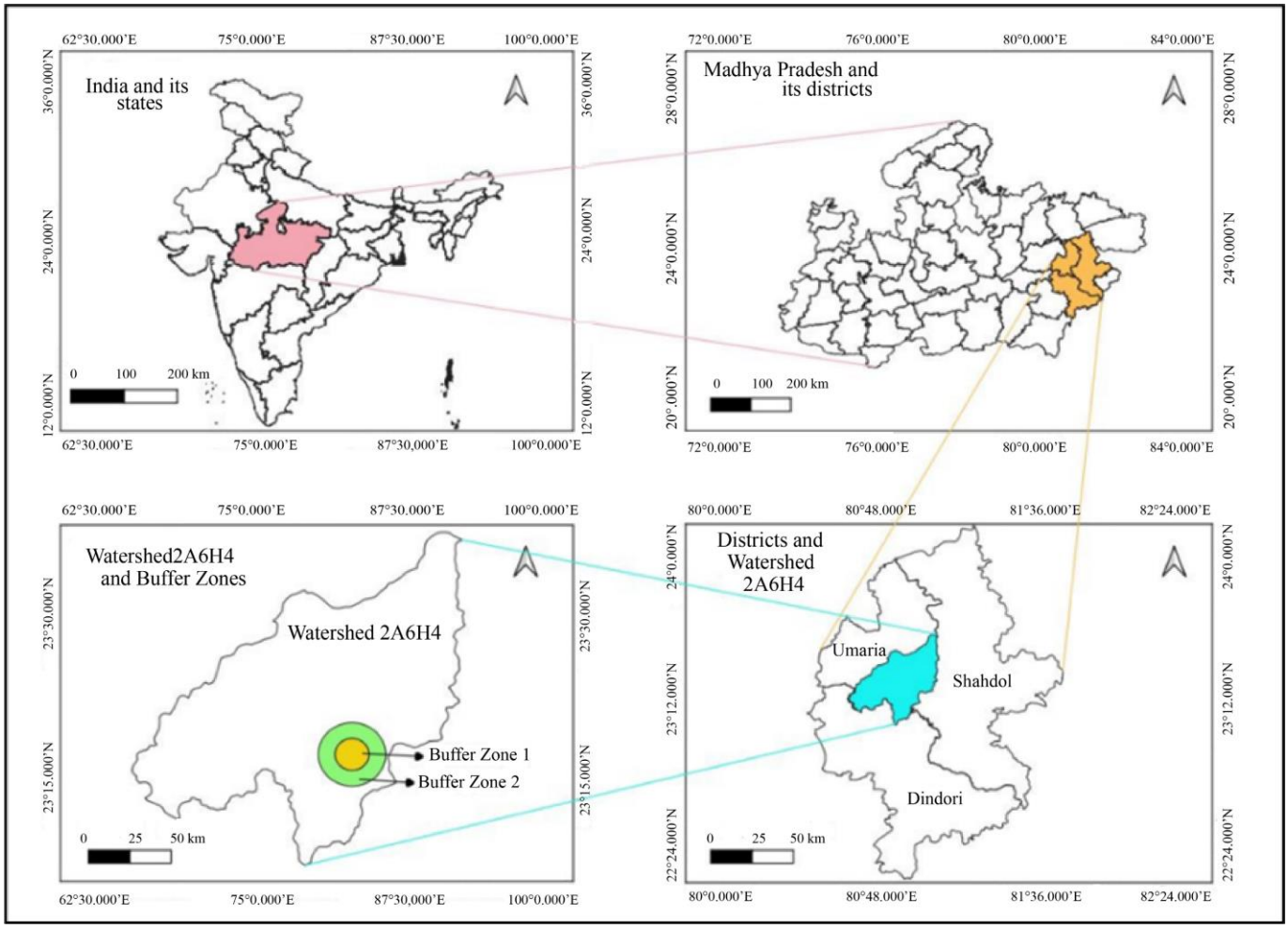


**Fig. 1 Location map of the study area**

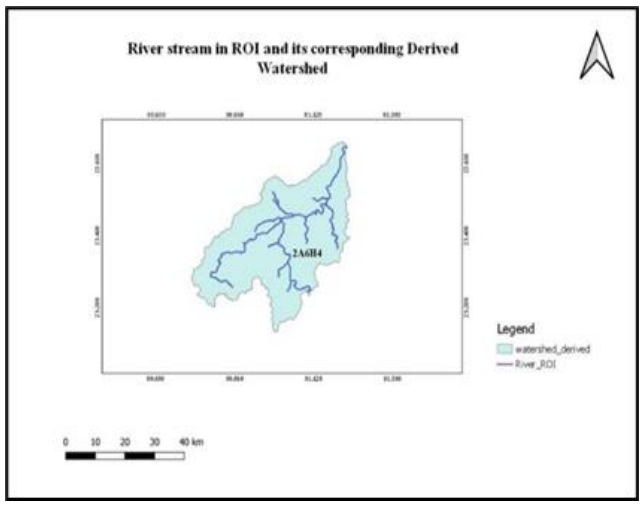


**Fig. 2 Derived Watershed and Study Area Using River Stream Lying in ROI**

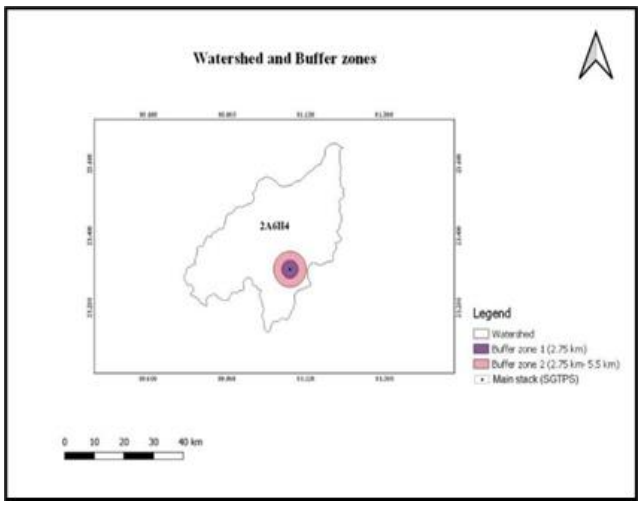


**Fig. 3 Buffer Zones Creation: Buffer 1 at a Radial Distance of 2.75 km and Buffer 2 at a Radial Distance of 2.75 km to 5.5 km Around SGTPS**

### *3.2. Supervised Classification and Estimation of Change in LULC*

Using Sentinel-2 data, Google Earth Engine (GEE) and Google Earth images, supervised classification was performed to find the LULC change in the ROI between October 2016 and October 2021.

Based on the investigation through Google Earth Images, the ROI is classified into six broad classes, namely Waterbody, Ash Pond, Forest, Built-up area, Barren land and Agricultural land, as shown in Figure 4.

### *3.3. Estimation of NDVI, LST, and SMI Indices Values for the Study Area*

Landsat-8 and Sentinel-2 satellite images for October 2016 and October 2021 containing the study area were obtained from the USGS EarthExplorer website [28]. Using QGIS software, these images were pre-processed to remove unwanted haze and cloud cover, which may lead to errors in analysis. [29] Some bands of the images were converted to top-of-the-atmosphere (TOA) radiance for the analysis.

Since the thermal power plants serve as heat centers, thus they may affect the land surface temperature and soil moisture of their surroundings, which in turn may affect the vegetation health, so it is essential to estimate the indices related to land surface temperatures and soil moisture such as LST and SMI respectively for the ROI and find the relationship between them and the vegetation health indicator index NDVI to get an idea about its impact on surrounding forest health. Thus, indices like the NDVI, LST, and SMI were estimated using pre-processed Landsat-8 satellite imagery for the ROI using the formulas given in Equation 1, 2, and 3, respectively. [20]

$$NDVI = \frac{(NIR-RED)}{(NIR+RED)} \quad (1)$$

Where RED is the value of the red band, and NIR is the value of the near-infrared band.

$$LST = \frac{BT}{[1+(\frac{\lambda * BT}{C_2}) * \ln \epsilon]} \quad (2)$$

Where *B.T.* is at-satellite Brightness Temperature, $\lambda$ is the wavelength of emitted radiance, $C_2$ is constant (1.4388 x$10^{-2}$ meter Kelvin), and $\epsilon$ is emissivity (typically 0.95).

$$SMI = \frac{(LST_{max}-LST)}{(LST_{max}-LST_{min})} \quad (3)$$

Where the maximum and minimum surface temperatures for a specific LST are denoted by $LST_{max}$ and $LST_{min}$. Then, correlation analysis is performed between *NDVI, LST* and *SMI* values to find a relationship between them for ROI.

Estimated values of NDVI, LST and SMI for two buffer zones for the years 2016 and 2021 are depicted in pictorial form through the following maps shown in Figures 5, 6, 7, 8, 9 and 10.

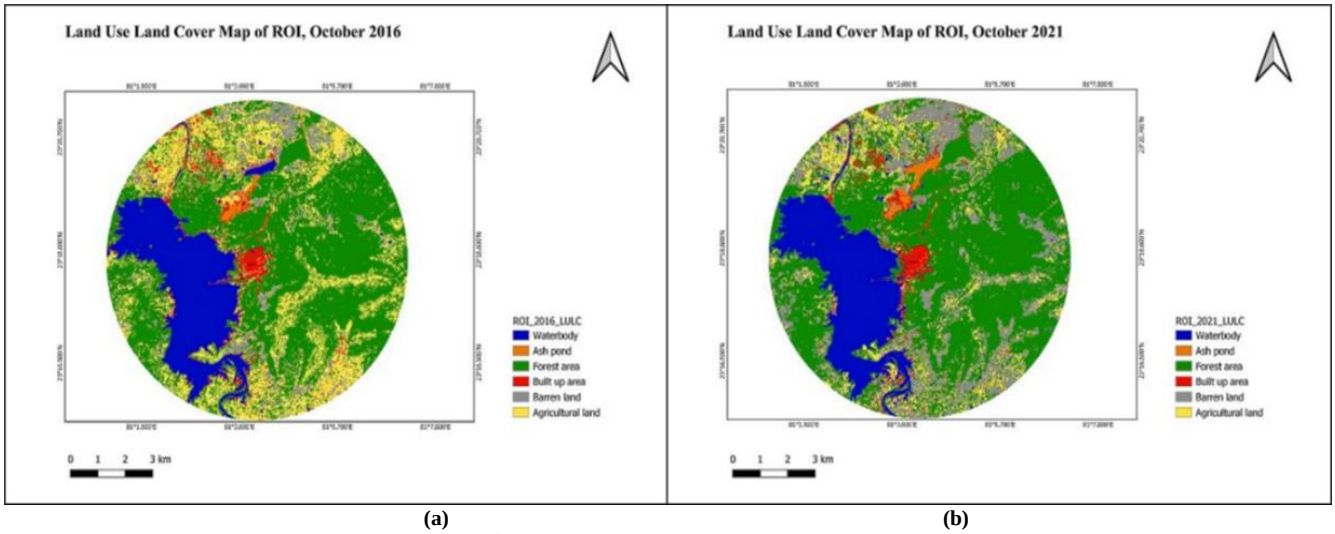


**(a)** **(b)**

**Fig. 4 LULC Maps for the Complete Study Area (a) October 2016, (b) October 2021**

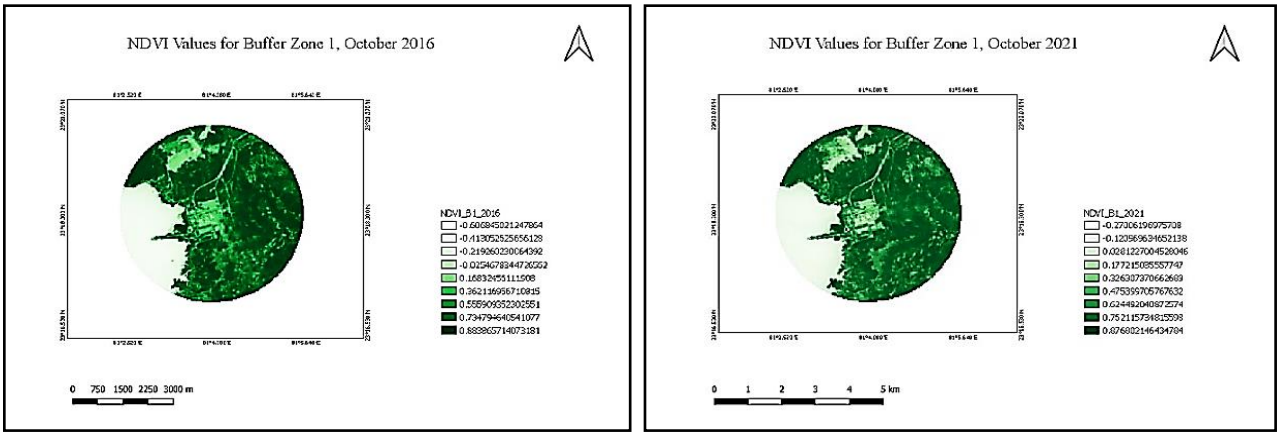


**(a)** **(b)**

**Fig. 5 NDVI Values for Buffer Zone 1 Estimated for October (a) 2016, (b) 2021**

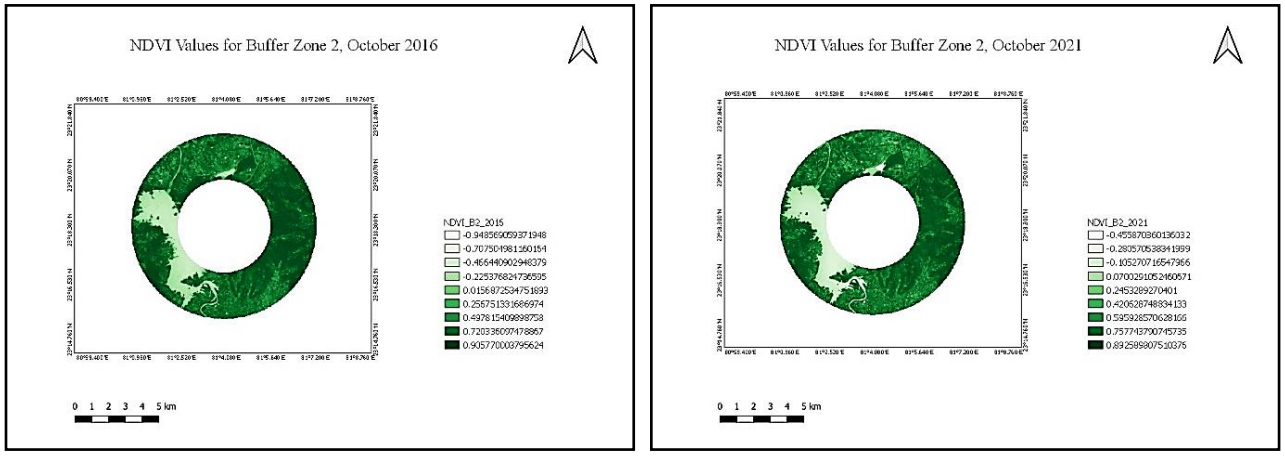


**(a)** **(b)**

**Fig. 6 NDVI Values for Buffer Zone 2 Estimated for October (a) 2016, (b) 2021**

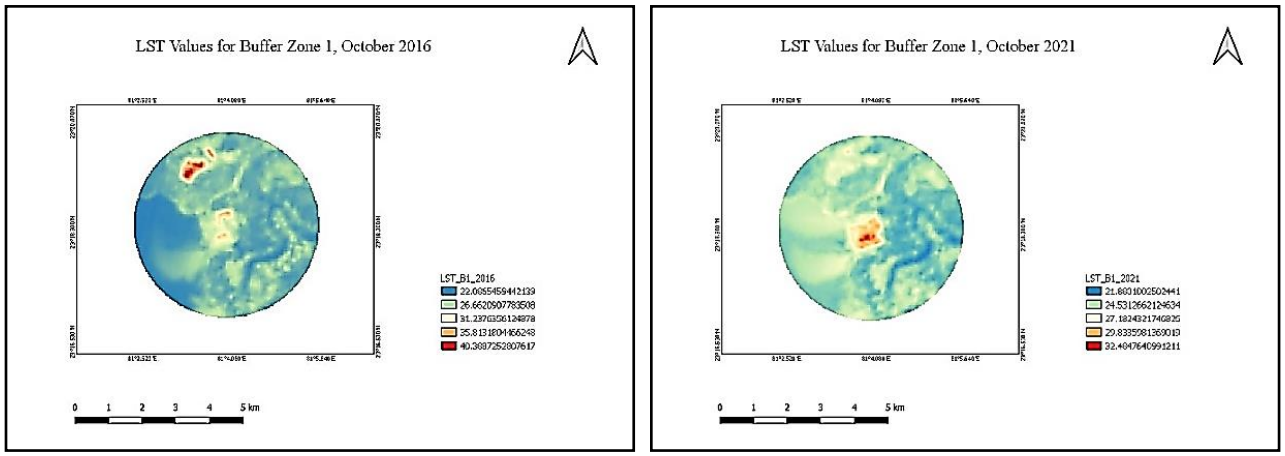


**(a)** **(b)**

**Fig. 7 LST Values for Buffer Zone 1 Estimated for October (a) 2016, (b) 2021**

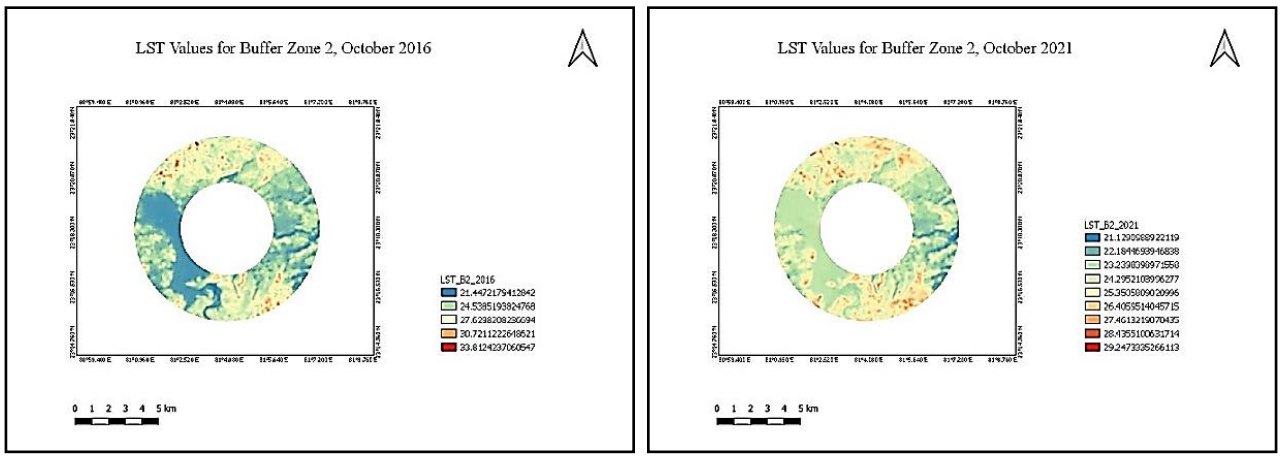


**(a)** **(b)**

**Fig. 8 LST values for buffer zone 2 estimated for october (a) 2016, (b) 2021**

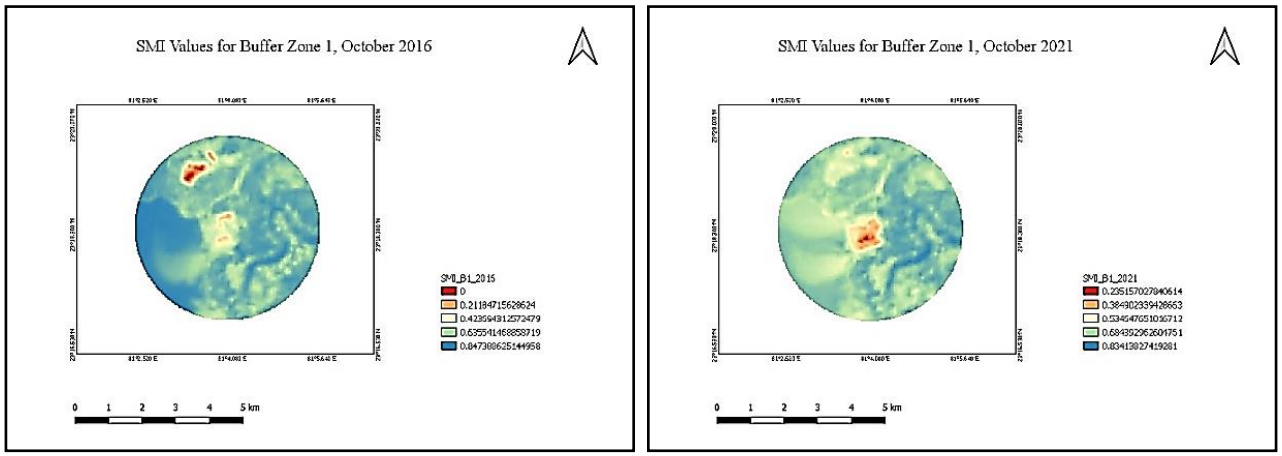


(a) (b)

**Fig. 9 SMI values for buffer zone 1 estimated for october (a) 2016, (b) 2021**

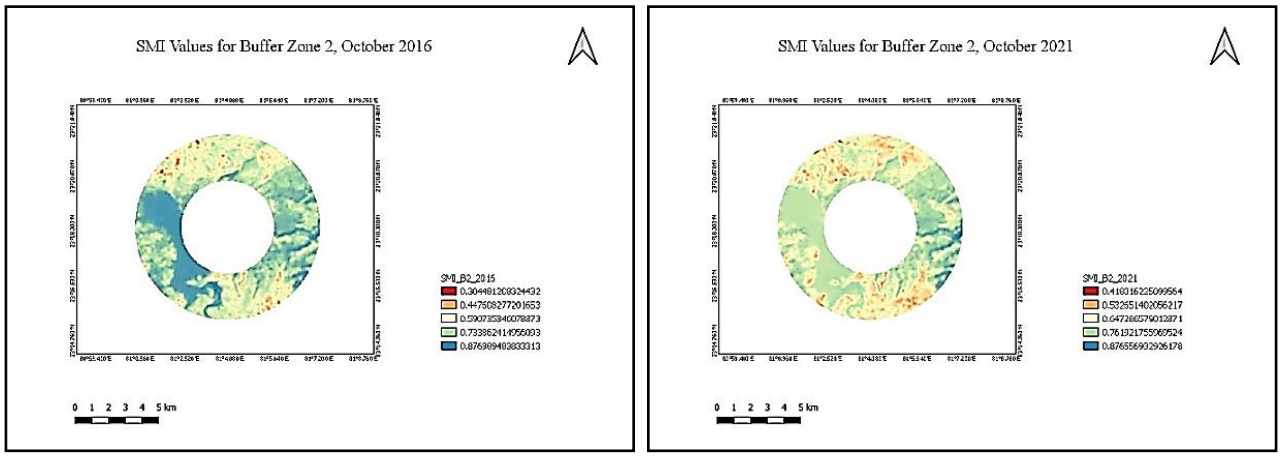


**(a)** **(b)**

**Fig. 10 SMI values for buffer zone 2 estimated for october (a) 2016, (b) 2021**

After estimating indices for complete ROI, some of these values at the same points within different buffer zones were randomly picked up and plotted in the form of a histogram in Figures 11, 12, 13, 14, 15 and 16.

Correlation analysis is performed over these estimated values of NDVI, LST, and SMI using a linear regression model, and respective relationship trends are obtained, which are discussed in Section 4.

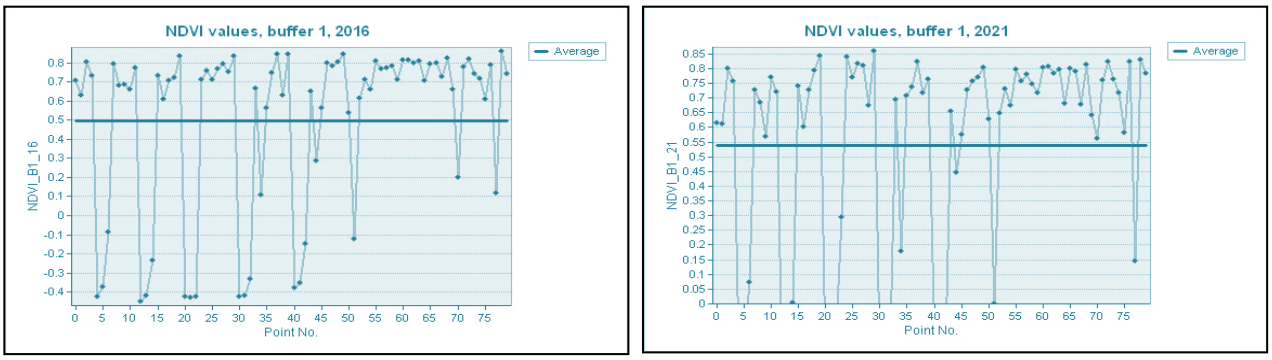


(a) (b)

**Fig. 11 Estimated NDVI Value Histogram for Buffer 1 in (a) 2016, (b) 2021**

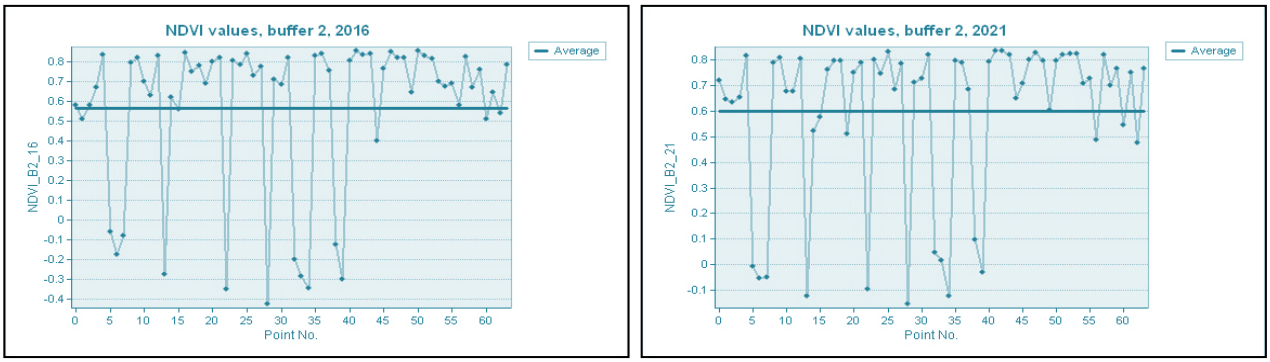


(a) (b)

**Fig. 12 Estimated NDVI Value Histogram for Buffer 2 in (a) 2016, (b) 2021**

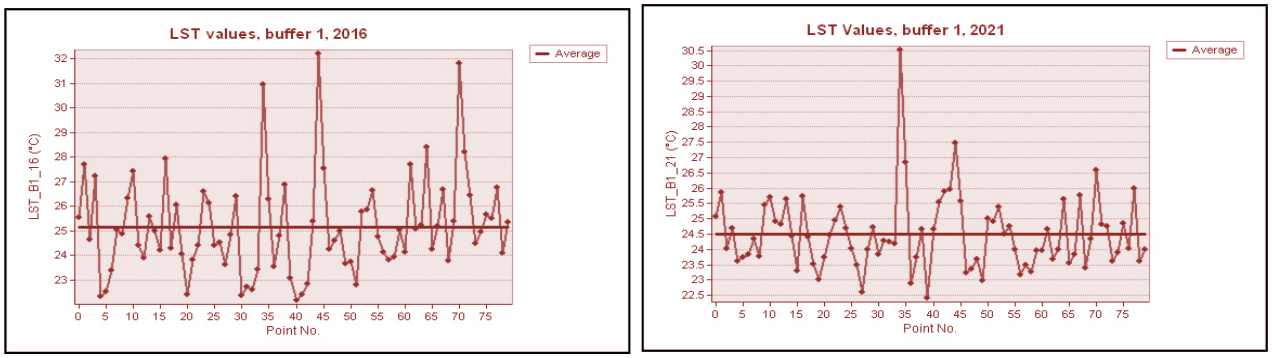


(a) (b)

**Fig. 13 Estimated LST Value Histogram for Buffer 1 in (a) 2016, (b) 2021**

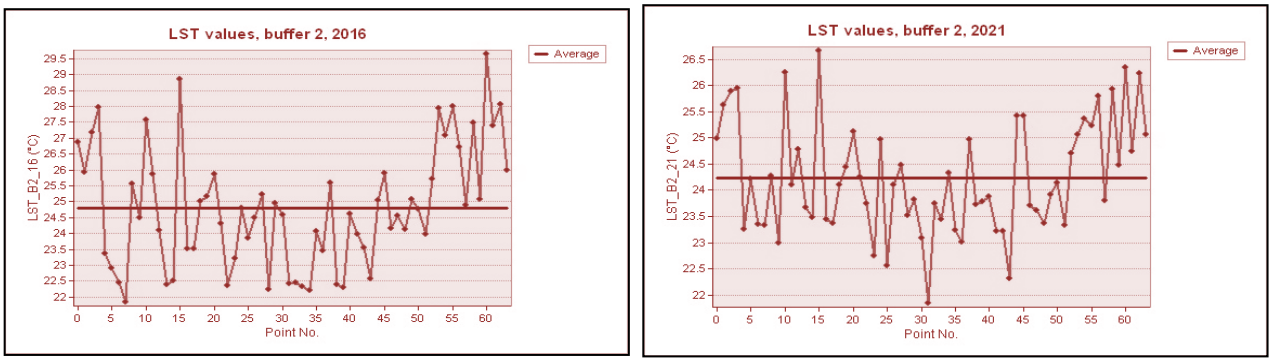


**(a) (b)**

**Fig. 14 Estimated LST Value Histogram for Buffer 2 in (a) 2016, (b) 2021**

### *3.4. Estimation of Monthly Mean Values of NDVI and Emitted Pollutants ($SO_2$, $NO_x$, PM, CO) by the SGTPS*

In order to explore the effect of the pollutants released by the TPPs on the health of the surrounding forest's vegetation, the relationship between the emitted pollutants and NDVI was explored. The monthly and yearly data for major emitted pollutants like $SO_2$, $NO_x$, PM, and CO were obtained from SGTPS, and the GEE tool was used to estimate the monthly and yearly mean of NDVI for ROI. Then, the link between NDVI and SGTPS's emitted pollutants in the study area was explored using correlation analysis, employing scatter plots. All the generated data have been appropriately validated after completion of all preceding stages, and the reasons for the apparent association and for the shift in LULC have been investigated. Finally, conclusions are drawn based on data, analysis and observations of local scenarios and practices being followed at SGTPS. Additionally, future recommendations have been provided. The methodology followed is visually represented in Figure 17.

## 4. Results and Analysis

### *4.1. Accuracy Assessment of Derived Watershed*

For the derived Watershed accuracy assessment, standard IWMP Watershed data (2A6H4) was used. Overlaying IWMP and derived watershed layers (Figure 18) revealed a 10.564 sq km difference, equating to a 0.696% error. The result obtained is summarized in Table 1. The derived watershed's accuracy came out to approximately 99.304%, considering the potential for boundary changes due to natural or anthropogenic factors.

### *4.2. Estimation of Change in LULC Based on Supervised Classification*

Based on the supervised LULC classification performed as mentioned under Section 3 and observing the obtained classification reports, an analysis is performed, and the following change in LULC is detected, as summarized in Table 2. The findings reveal that the reduction in waterbody areas can be majorly ascribed to the expansion of ash pond areas, and other possible causes can be sedimentation, inadequate cleaning practices, or desiccation of water bodies. The augmentation of built-up areas can be linked to increased human habitation and industrialization.

A noteworthy surge in the ash pond's area implies increased water contamination due to the deposition of waste ash. The expansion of forested areas suggests a lack of significant adverse impacts from the SGTPS.

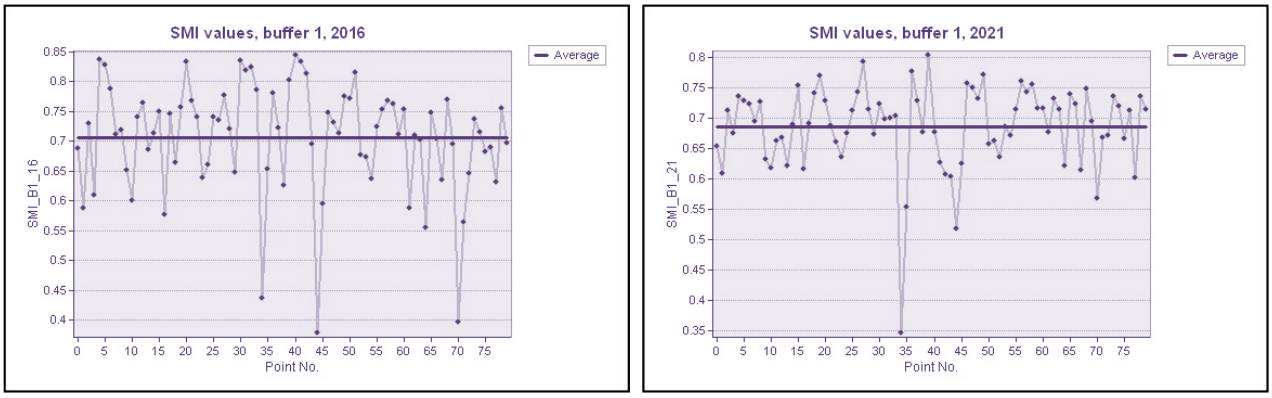


**(a)** **(b)**

**Fig. 15 Estimated SMI Value Histogram for Buffer 1 in (a)2016, (b) 2021**

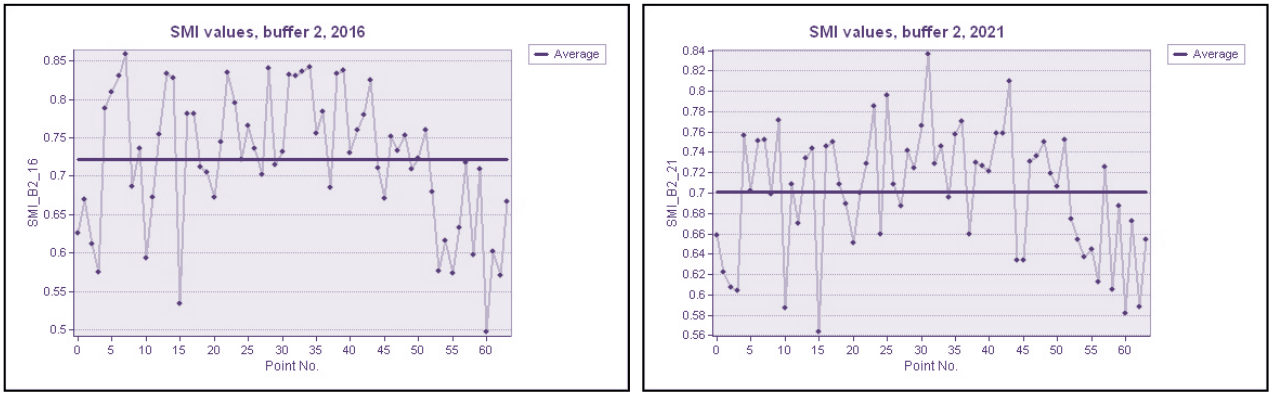


**(a)** **(b)**

**Fig. 16 Estimated SMI Value Histogram for Buffer 2 in (a) 2016, (b) 2021**

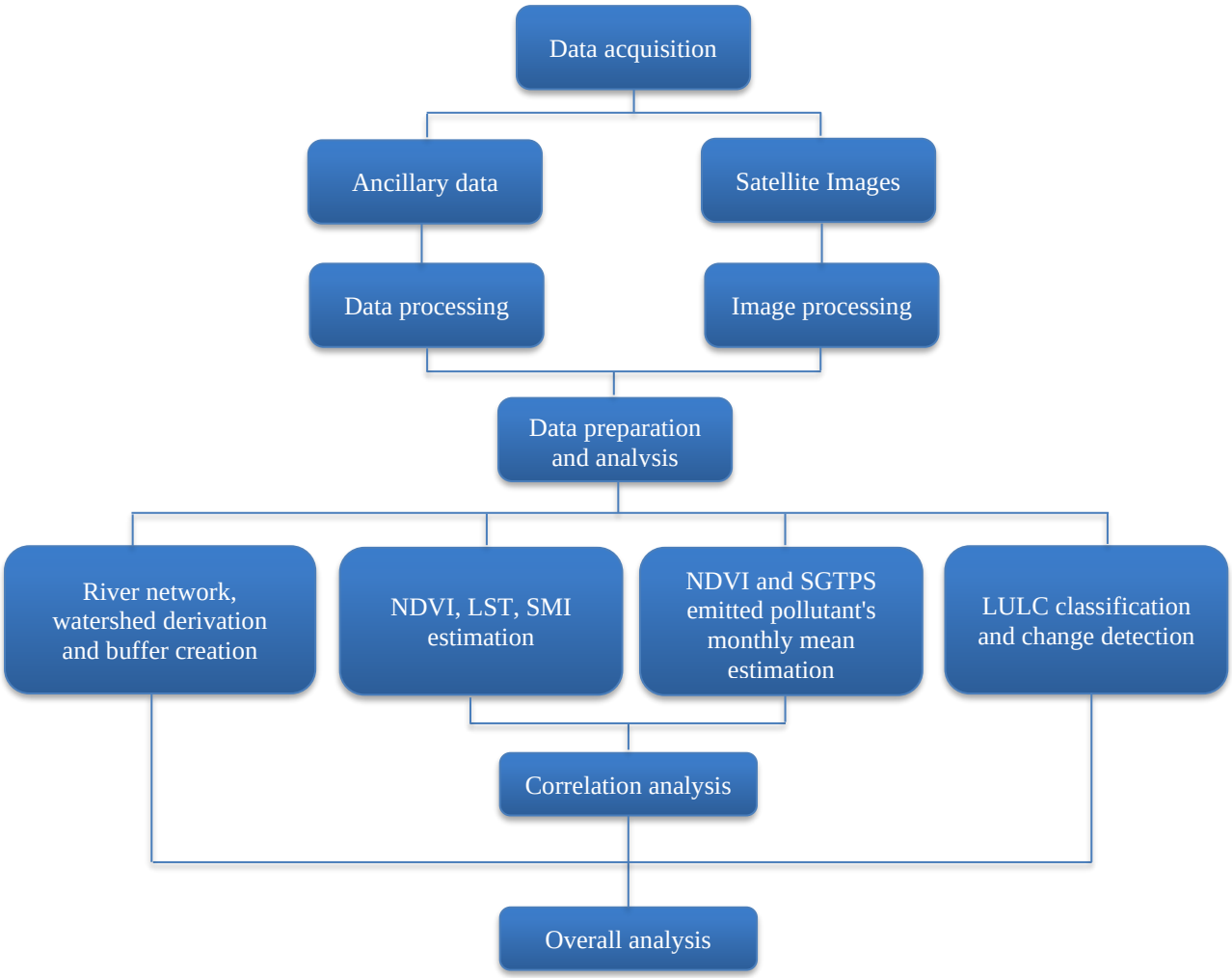


**Fig. 17 Flowchart of methodology**

**Table 1. Difference between derived and standard watershed**

| S. No. | Name of watershed | Area ($km^2$) | Change in the area ($km^2$) | % error in the area |
|---|---|---|---|---|
| **1.** | IWMP watershed 2A6H4 | 1517.723 | -10.564 | -0.696 |
| **2** | Derived watershed | 1507.159 | | |

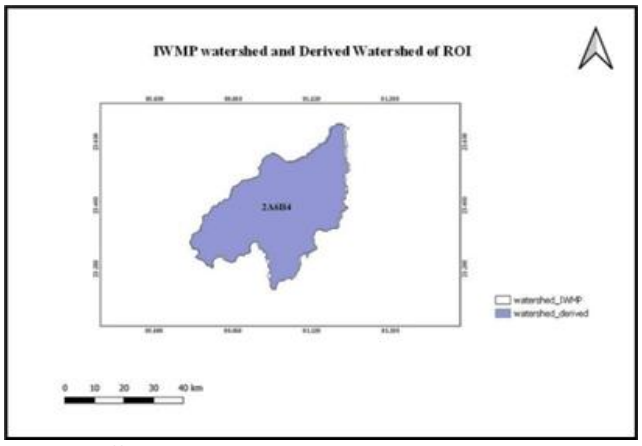


**Fig. 18 Difference Between IWMP Standard Watershed and Derived Watershed for ROI**

However, the COVID-19 lockdown, which caused the cessation of anthropogenic activities, emerges as a noteworthy factor contributing to the restoration of natural conditions and improvements in the climate. [18] The decline in agricultural land and the rise in barren land may be attributed to the COVID-19 lockdown, or other factors can be the migration of individuals to urban centers in pursuit of enhanced educational opportunities for their children and employment.

Although good accuracy is obtained in classification, due to the COVID-19 pandemic, both training and validation for classification were based on the comparison between the classified satellite imagery and Google Earth images only, which limited its accuracy compared to in-situ observations.

### *4.3. Correlation Analysis of Estimated Values of NDVI, LST, and SMI for the Study Area*

LST and SMI can be associated with SGTPS activity since they operate as heat centers. Thus, their inclusion in the study is crucial. The estimation of all three indices, namely NDVI, LST and SMI, at different points in ROI, is already explained in Section 3.

Correlation analysis is performed over the estimated values of NDVI, LST and SMI using a linear regression model and respective relationship trends obtained, which are represented in Figures 19, 20, 21, 22, 23 and 24. Based on these, as summarized in Table 3, NDVI and LST exhibit a direct association in buffer zone 1 but an inverse relationship in buffer zone 2 for 2016 and 2021. According to most of the literature, NDVI and LST have a negative relationship, [18,30] but according to some specific research publications, [19,20,31] NDVI and LST can have a positive relationship based on the season of observation. The recorded ranges of LST and SMI in buffer zones establish typical temperature and SMI levels. Consequently, despite the thermal power plant's activity, the impact on LST and SMI is minimal, ensuring the stability of vegetation health, particularly in forests.

**Table 2. Change in LULC from October 2016 to October 2021**

| S.No. | Class | Area in 2016 (sq Km) | Area in 2021 (sq Km) | Percentage change in area |
|---|---|---|---|---|
| 1 | Waterbody | 16.1875 | 15.6678 | -3.21 |
| 2 | Ash pond | 0.7623 | 0.7867 | 3.20 |
| 3 | Forest | 42.6873 | 43.4642 | 1.82 |
| 4 | Built-up area | 5.3871 | 5.4937 | 1.98 |
| 5 | Barren land | 5.1455 | 5.2232 | 1.51 |
| 6 | Agricultural land | 22.8918 | 22.3699 | -2.28 |

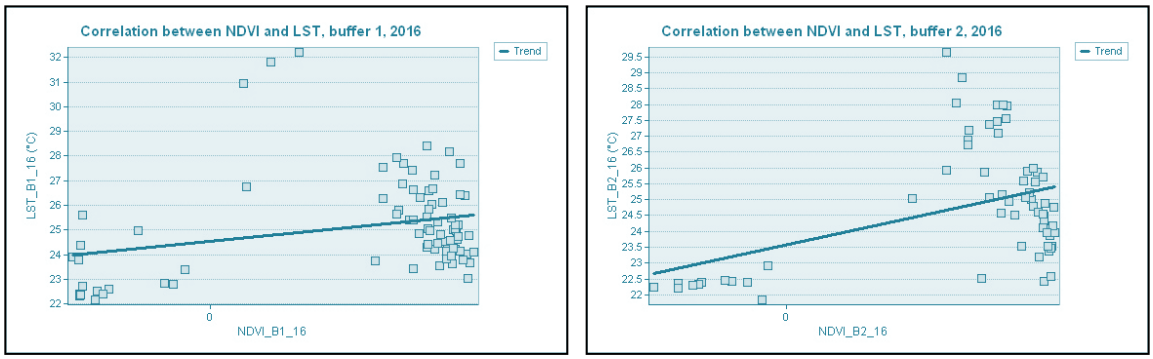


**(a)** **(b)**

**Fig. 19 Estimated Scatter Plot Between NDVI and LST Values for 2016 in Buffer 1 (a) and Buffer 2 (b).**

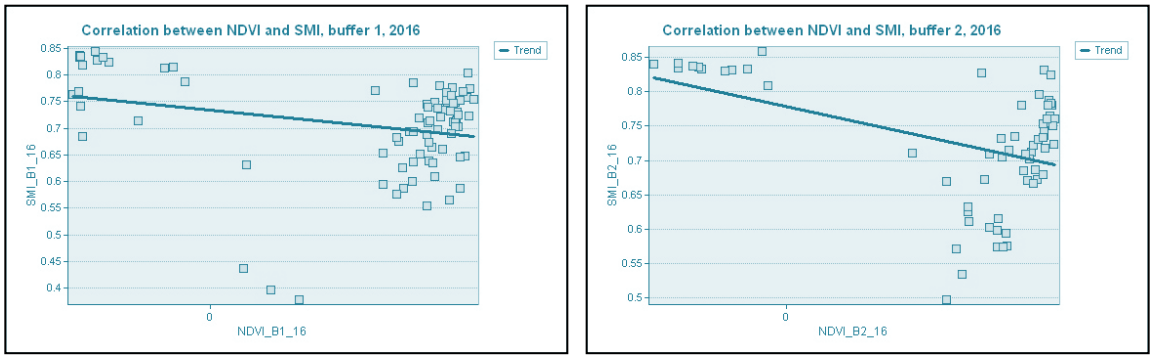


**(a)** **(b)**

**Fig. 20 Estimated Scatter Plot Between NDVI and SMI Values for 2016 in Buffer 1 (a) and Buffer 2 (b).**

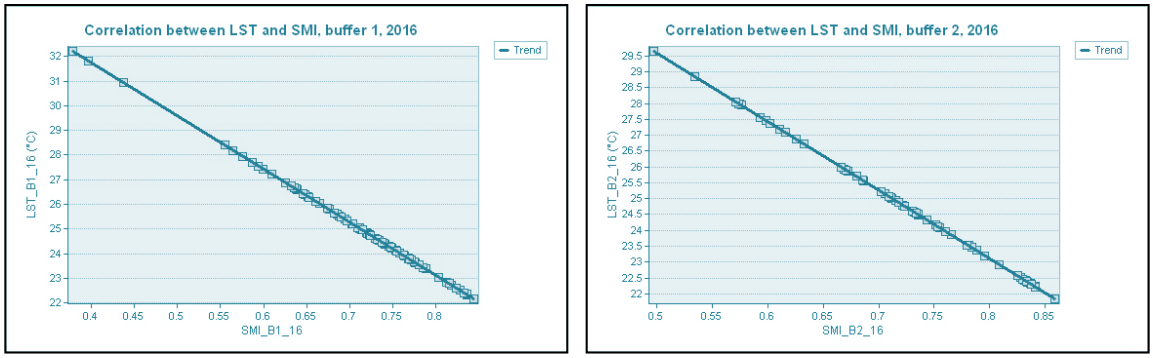


**(a)** **(b)**

**Fig. 21 Estimated Scatter Plot Between SMI and LST Values for 2016 in Buffer 1 (a) and Buffer 2 (b).**

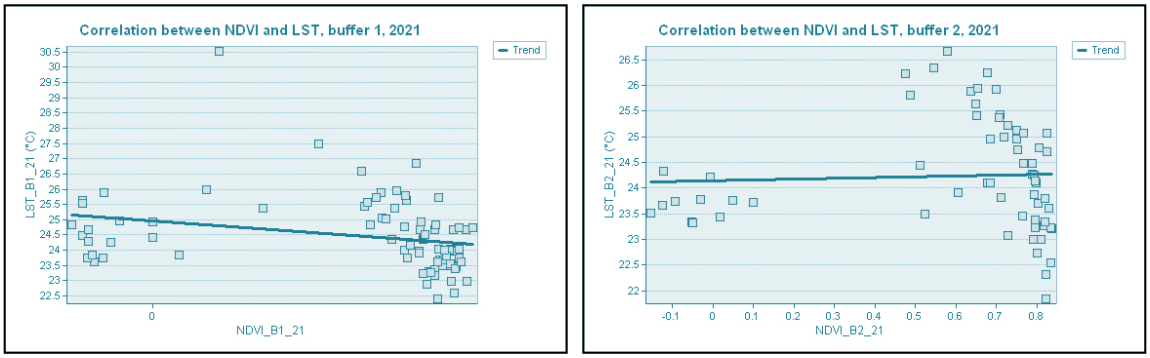


**(a)** **(b)**

**Fig. 22 Estimated Scatter Plot Between NDVI and LST Values for 2021 in Buffer 1 (a) and Buffer 2 (b).**

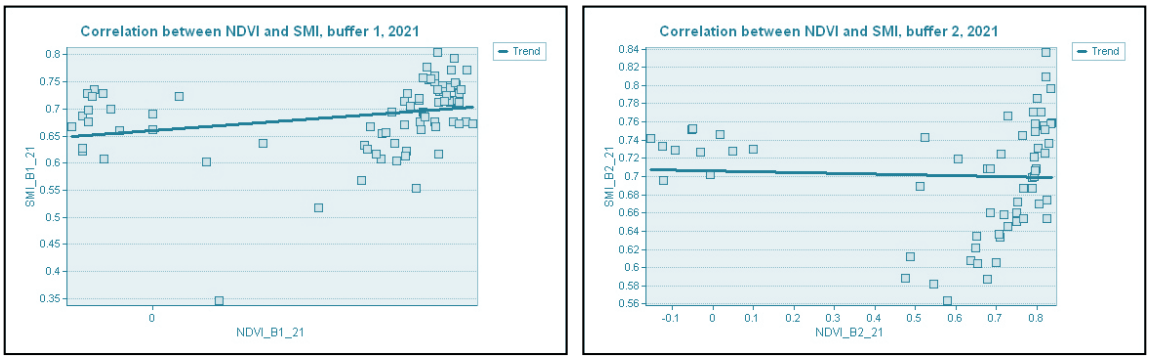


**(a)** **(b)**

**Fig. 23 Estimated Scatter Plot Between NDVI and SMI Values for 2021 in Buffer 1 (a) and Buffer 2 (b).**

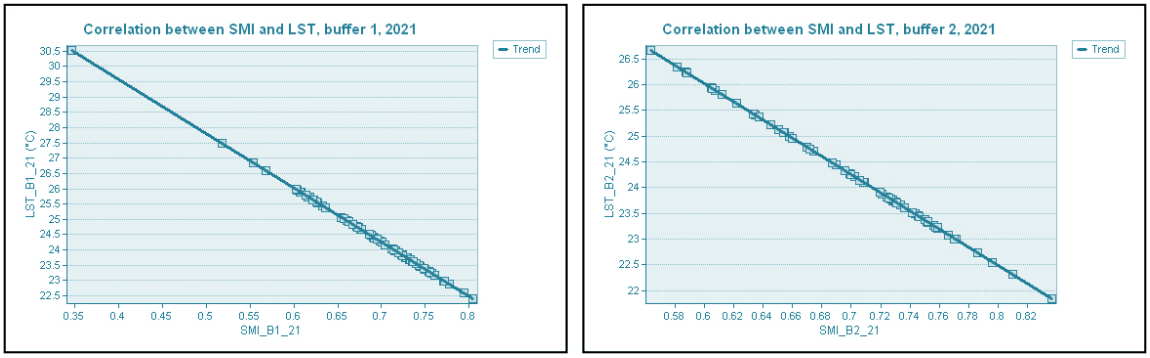


**(a)** **(b)**

**Fig. 24 Estimated Scatter Plot Between SMI and LST Values for 2021 in Buffer 1 (a) and Buffer 2 (b).**

**Table 3. Relationship Between NDVI, LST and SMI for Both Buffer Zones for Oct 2016 and Oct 2021**

| Buffer | | October 2016 | | | | October 2021 | | |
|---|---|---|---|---|---|---|---|---|
| | Relationship | NDVI | LST | SMI | Relationship | NDVI | LST | SMI |
| Buffer1 | NDVI | Perfect Positive | Positive | Negative | NDVI | Perfect Positive | Negative | Positive |
| | LST | Positive | Perfect Positive | Perfect Negative | LST | Negative | Perfect Positive | Perfect Negative |
| | SMI | Negative | Perfect Negative | Perfect Positive | SMI | Positive | Perfect Negative | Perfect Positive |
| Buffer2 | NDVI | Perfect Positive | Positive | Negative | NDVI | Perfect Positive | Positive | Negative |
| | LST | Positive | Perfect Positive | Perfect Negative | LST | Positive | Perfect Positive | Perfect Negative |
| | SMI | Negative | Perfect Negative | Perfect Positive | SMI | Negative | Perfect Negative | Perfect Positive |

### *4.4. Correlation Analysis of Estimated Monthly Mean Values of NDVI and Emitted Pollutants ($SO_2$, $NO_x$, PM, CO) by the SGTPS*

This study employs correlation analysis to assess the impact of pollutants from SGTPS on the surrounding forest. Results of the correlation between different emitted pollutants of SGTPS with the mean NDVI values for respective buffer zones for the years 2016 and 2021 are summarized in Table 4. Results show that pollutants emitted by the SGTPS have a modest negative relationship with NDVI, as suggested by the slope of linear regression, as pollutant levels align with CPCB standards. [32] Some instances exhibit a positive correlation, suggesting limited adverse effects on forest health. For such exceptional cases, factors like rainfall, [33] wind speed and direction, [34] extent of fly ash deposition on foliage, [35] and reduced anthropogenic activities during the COVID-19 pandemic can be potential influencers, [18] forming the study's scope. Following scatter plots obtained during linear regression analysis as shown in Figures 25, 26, 27, 28, 29, 30, 31 and 32.

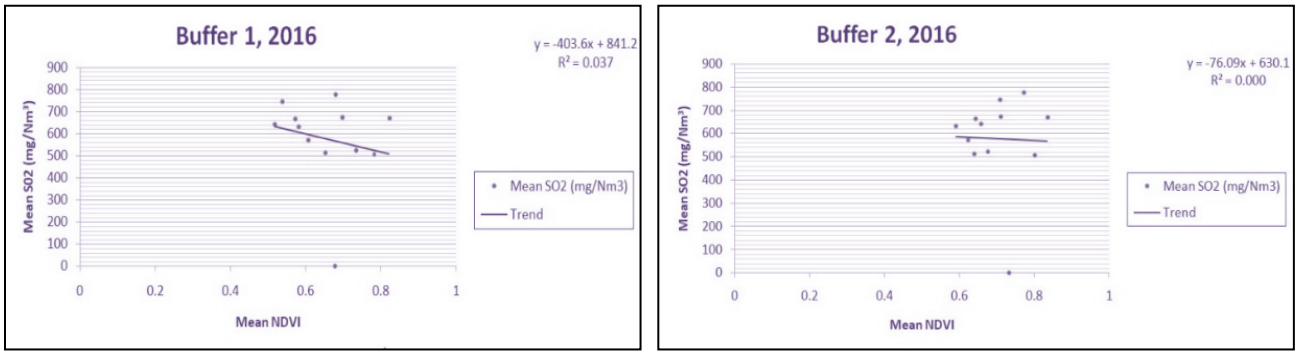


**(a)** **(b)**

**Fig. 25 Correlation Between emitted SO2 and NDVI values for 2016 Buffer 1 (a) and Buffer 2 (b).**

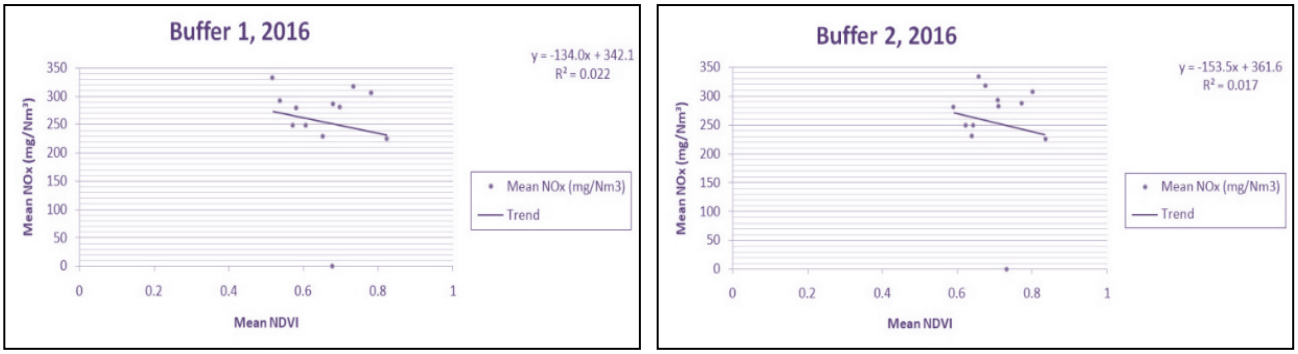


**(a)** **(b)**

**Fig. 26 Correlation between emitted NOx and NDVI values for 2016 Buffer 1 (a) and Buffer 2 (b).**

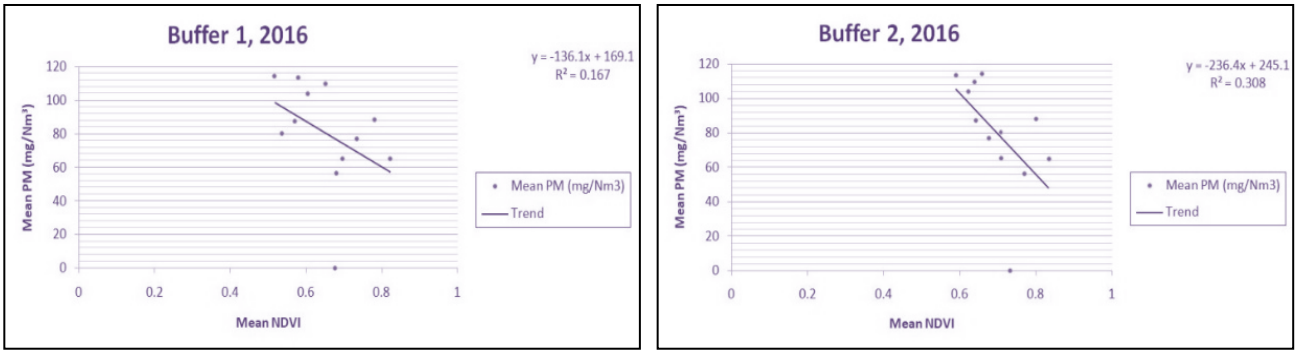


**(a)** **(b)**

**Fig. 27 Correlation between emitted PM and NDVI values for 2016 Buffer 1 (a) and Buffer 2 (b).**

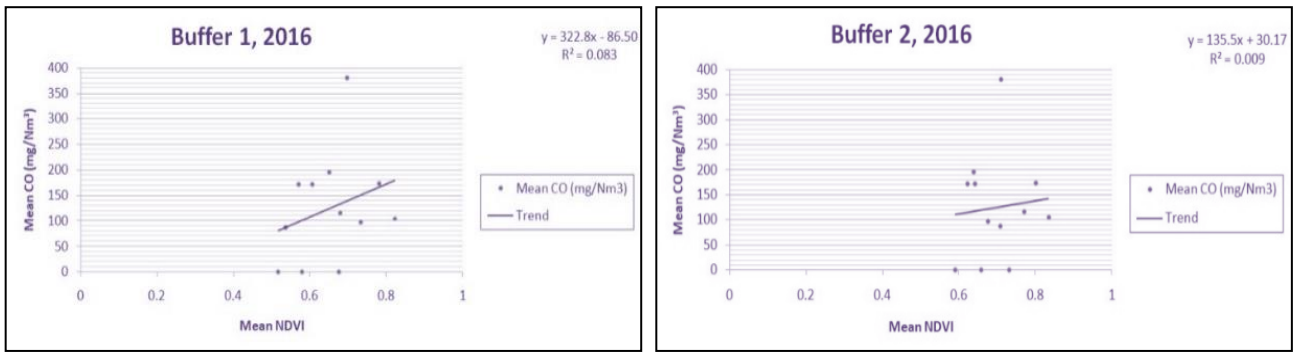


**(a)** **(b)**

**Fig. 28 Correlation between emitted CO and NDVI values for 2016 Buffer 1 (a) and Buffer 2 (b).**

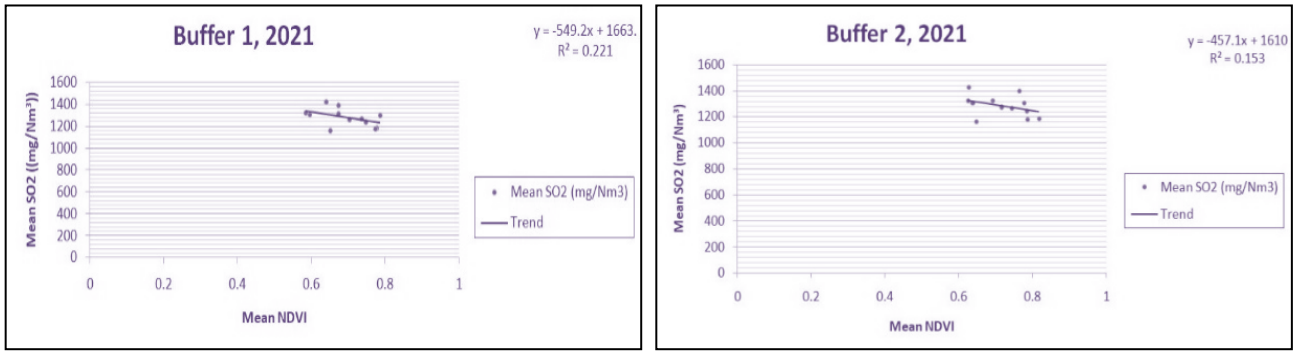


**(a)** **(b)**

**Fig. 29 Correlation between emitted SO2 and NDVI values for 2021 Buffer 1 (a) and Buffer 2 (b).**

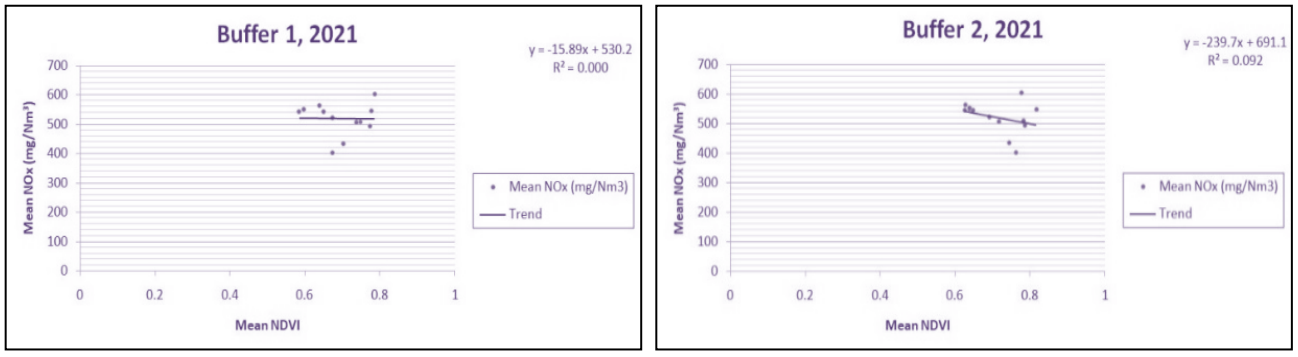


**(a)** **(b)**

**Fig. 30 Correlation between emitted NOx and NDVI values for 2021 Buffer 1 (a) and Buffer 2 (b).**

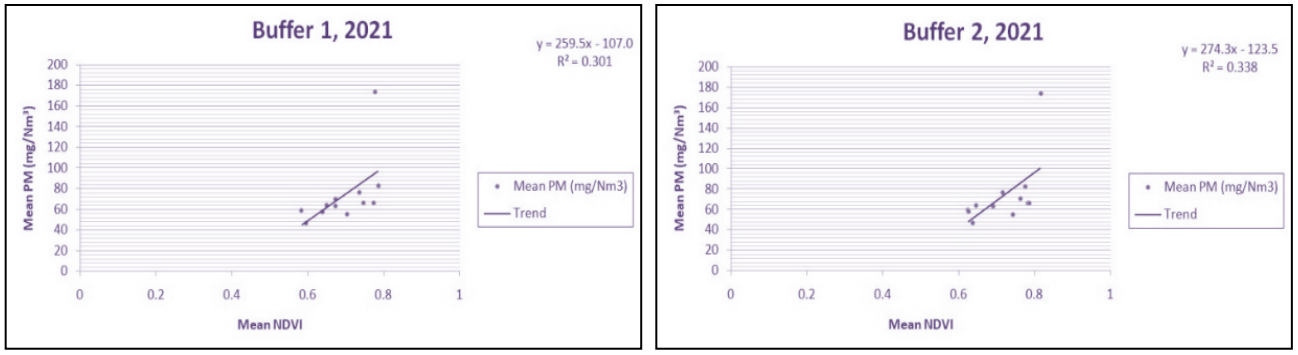


**(a)** **(b)**

**Fig. 31 Correlation between emitted PM and NDVI values for 2021 Buffer 1 (a) and Buffer 2 (b).**

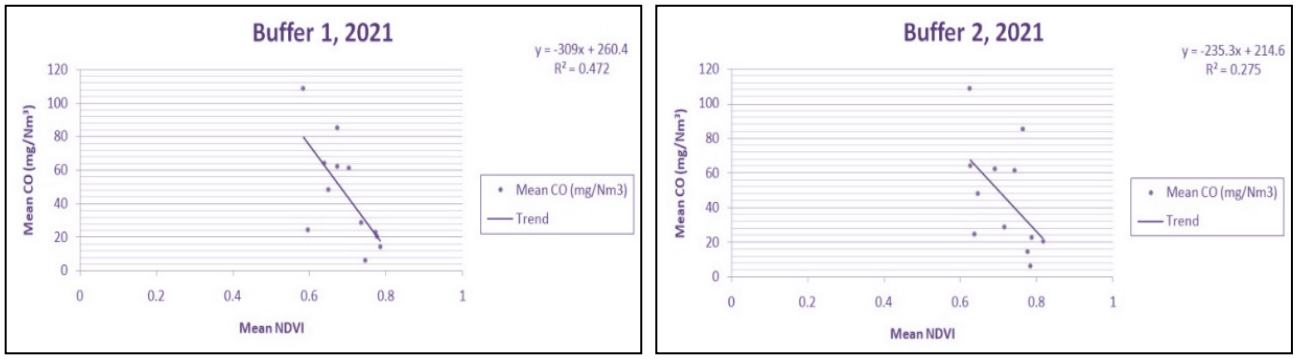


**(a)** **(b)**

**Fig. 32 Correlation between emitted CO and NDVI values for 2021 Buffer 1 (a) and Buffer 2 (b).**

**Table 4. Relationship (Correlation coefficient) between Mean NDVI and pollutants emitted by SGTPS for both buffer zones for 2016 and 2021**

| Pollutant | Mean NDVI (Buffer 1, 2016) | Mean NDVI (Buffer 2, 2016) | Mean NDVI (Buffer 1, 2021) | Mean NDVI (Buffer 2, 2021) |
|---|---|---|---|---|
| $SO_2$ | Negative (-0.294) | Positive (0.229) | Negative (-0.47) | Negative (-0.392) |
| $NO_x$ | Negative (-0.209) | Negative (-0.01) | Negative (-0.02) | Negative (-0.303) |
| PM | Negative (-0.571) | Negative (-0.73) | Positive (0.549) | Positive (0.581) |
| CO | Positive (0.017) | Negative (-0.199) | Negative (-0.687) | Negative (-0.524) |

## 5. Conclusion

In conclusion, this study utilized a simple method based on RS and GIS to assess the impact of SGTPS on surrounding forests, focusing on LULC changes and the correlation of forest vegetation health indication index (NDVI) with emitted pollutants, LST and SMI, which is one of its prominent features which distinguishes it with other studies conducted so far who focused on only one aspect and are complex [22-26]. In contrast to [30], the usage of good-resolution satellite datasets such as Sentinel-2 datasets in this study helped to overcome the limitation of poor resolution. Overall, the study has shown an increase in forest area, which indicates there was not much deforestation or damage to the vegetation. It has been found that the values for the indices and pollutant levels lie within the suggested limit by the CPCB and show adherence to government norms. The relationships between the NDVI and other indices and pollutants are primarily in line with the literature, except for a few that need more investigation. Although it has been concluded that the emitted pollutants affected forest health, it is clear from the plots and correlation coefficients that no severe impact was exhibited, possibly attributed to the pollution mitigation practices of SGTPS. The findings show the potential of RS and GIS for effective monitoring, analysis, policy formulation, and improved management of thermal power plants and forests.

## Data Availability Statement

Satellite data used for deriving watershed, LULC change detection, and indices estimation are available at the USGS EE website at https://earthexplorer.usgs.gov [28]. Data related to

SGTPS supporting the findings of this study is confidential and can be obtained at the request of the concerned authorities at SGTPS, Birsinghpur Pali, Madhya Pradesh, India.

## Acknowledgements

The authors would like to acknowledge Mr. Pankaj Jain (Superintending Engineer, ETI-2), Smt. Divya Tiwari (Senior Chemist, SGTPS MPPGCL), thank you for providing valuable information about the SGTPS. We thank Dr Suresh Band Goswami and Mr Shardendu Shukla for their unwavering technical assistance. We extend heartfelt gratitude to the Department of Civil Engineering, MANIT Bhopal, for providing all the necessary facilities for conducting this study.

## References

[1] Ministry of Coal, Government of India Website. [Online]. Available: https://coal.nic.in/en/major-statistics/generation-of-thermal-power-from-raw-coal

[2] Anita Singh, and Madhoolika Agrawal, "Acid Rain and Its Ecological Consequences," *Journal of Environmental Biology*, vol. 29, no. 1, pp. 15– 24, 2008. [Google Scholar]

[3] Rafid M. Hannun, and Ali H. Abdul Razzaq, "Air Pollution Resulted from Coal, Oil and Gas Firing in Thermal Power Plants and Treatment: A Review," *IOP Conference Series: Earth and Environmental Science*, vol. 1002, 2022. [CrossRef] [Google Scholar] [Publisher Link]

[4] Christian Ulrichs et al., "Effect of Solid Particulate Matter Deposits on Vegetation: A Review," *Functional Plant Science and Biotechnology*, vol. 2, no. 1, pp. 56-62, 2008. [Google Scholar]

[5] Yifan Li et al., "The response of Plant Photosynthesis and Stomatal Conductance to Fine Particulate Matter (pm 2.5) based on Leaf Factors Analyzing," *Journal of Plant Biology*, vol. 62, pp. 120–128, 2019. [CrossRef] [Google Scholar] [Publisher Link]

[6] M. Dogan Kantarci, "The Effects of Three Thermo Electric Power Plants on Yerkesik-denizova Forests in Mugla Province (Turkey)," *Water, Air, & Soil Pollution: Focus*, vol. 3, pp. 205– 213, 2003. [CrossRef] [Google Scholar] [Publisher Link]

[7] Averil Wilson, Shona Magill, and Kenny Black, "Review of Environmental Impact Assessment and Monitoring in Salmon Aquaculture," *FAO Fisheries and Aquaculture Technical Paper. No. 527.: Environmental Impact Assessment and Monitoring in Aquaculture*, pp. 455–535, 2009. [Google Scholar] [Publisher Link]

[8] Environmental Impact Assessment Advantages and Disadvantages, 2023. [Online]. Available: https://cypressei.com/engineering/environmental-impact-assessment-advantages-disadvantages/

[9] Natural Resources Canada website, Fundamentals of Remote Sensing – Introduction. [Online]. Available: https://natural-resources.canada.ca/maps-tools-and-publications/satellite-imagery-elevation-data-and-air-photos/tutorial-fundamentals-remote-sensing/introduction/9363/

[10] P.S. Roy, and Shirish A. Ravan, "Biomass Estimation using Satellite Remote Sensing Data—An Investigation on Possible Approaches for Natural Forest," *Journal of Biosciences*, vol. 21, pp. 535– 561, 1996. [CrossRef] [Google Scholar] [Publisher Link]

[11] K.E. Percy, and M. Ferretti, "Air Pollution and Forest Health: Toward New Monitoring Concepts," *Environmental Pollution*, vol. 130, no. 1, pp. 113– 126, 2004. [CrossRef] [Google Scholar] [Publisher Link]

[12] Alex M. Lechner, Giles M. Foody, and Doreen S. Boyd, "Applications in Remote Sensing to Forest Ecology and Management," *One Earth*, vol. 2, no. 5, pp. 405– 412, 2020. [CrossRef] [Google Scholar] [Publisher Link]

[13] Aneta Modzelewska, Fabian Ewald Fassnacht, and Krzysztof Steren'czak, "Tree Species Identification within an Extensive Forest Area with Diverse Management Regimes using Airborne Hyperspectral Data," *International Journal of Applied Earth Observation and Geoinformation*, vol. 84, p. 101960, 2020. [CrossRef] [Google Scholar] [Publisher Link]

[14] Harshika A. Kaul, and Ingle Sopan, "Land use Land Cover Classification and Change Detection using High Resolution Temporal Satellite Data," *Journal of Environment*, vol. 1, no. 4, pp. 146– 152, 2012. [Google Scholar]

[15] Eman A. Alshari, and Bharti W. Gawali, "Development of Classification System for LULC using Remote Sensing and GIS," *Global Transitions Proceedings*, vol. 2, no. 1, pp. 8–17, 2021. [CrossRef] [Google Scholar] [Publisher Link]

[16] R.R. Okhandiar, P.L.N. Raju, and Witzke Bijker, "*Neighbourhood Correlation Image Analysis Technique for Change Detection in Forest Landscape*," ITC, 2007. [Google Scholar]

[17] Dinh Thi Kim Phuong, Mai Cong Nhut, and Nguyen Duc Tri, "Air Pollution Assessment using RS and GIS in Ho Chi Minh City, Viet Nam: A Case Study of Period 2015- 2019 for SO2 and NO2," *IOP Conference Series: Earth and Environmental Science*, vol. 652, 2021. [CrossRef] [Google Scholar] [Publisher Link]

[18] Nurwita Mustika Sari, and Muhammad Nur Sidiq Kuncoro, "Monitoring of Co, No2 and So2 Levels During the Covid-19 Pandemic in Iran using Remote Sensing Imagery," *Geography, Environment, Sustainability*, vol. 14, no. 4, pp. 183–191, 2021. [CrossRef] [Google Scholar] [Publisher Link]

[19] Donglian Sun, and Menas Kafatos, "Note on the NDVI-LST Relationship and The use of Temperature-related Drought Indices over North America," *Geophysical Research Letters*, vol. 34, no. 24, 2007. [CrossRef] [Google Scholar] [Publisher Link]

[20] Arnab Saha et al., "Assessment and Impact of Soil Moisture Index in Agricultural Drought Estimation using Remote Sensing and GIS Techniques," *Proceedings*, vol. 7, no. 1, p. 2, 2019. [CrossRef] [Google Scholar] [Publisher Link]
[21] Sha Huang et al., "A Commentary Review on the Use of Normalized Difference Vegetation Index (NDVI) in the Era of Popular Remote Sensing," *Journal of Forestry Research*, vol. 32, pp. 1–6, 2021. [CrossRef] [Google Scholar] [Publisher Link]
[22] Ismail Mondal et al., "Modeling of Environmental Impact Assessment of Kolaghat Thermal Power Plant Area, West Bengal, using Remote Sensing and GIS Techniques," *Modeling Earth Systems and Environment*, vol. 2, 2016. [CrossRef] [Google Scholar] [Publisher Link]
[23] P. Padmavathi, Jyotsna Cherukuri, and M. Anji Reddy, "Ambient Air Pollutant Levels in the Vicinity of NTTPS Thermal Power Plant," *IOSR Journal of Environmental Science, Toxicology and Food Technology*, vol. 9, no. 2, pp. 56– 60, 2015. [CrossRef] [Google Scholar]
[24] Abdullah Harun Chowdhury, "Environmental Impact of Coal-based Power Plant of Rampal on the Sundarbans (World Largest Mangrove Forest) and Surrounding Areas," *MOJ Ecology and Environment Science*, vol. 2, no. 3, 2017. [Google Scholar]
[25] Sudhir Yadav, and Rajiv Prakash, "Status and Environmental Impact of Emissions from Thermal Power Plants in India," *Environmental Forensics*, vol. 15, no. 3, pp. 219–224, 2014. [CrossRef] [Google Scholar] [Publisher Link]
[26] Maya Kumari, and Kiranmay Sarma, "Changing Trends of Land Surface Temperature in Relation to Land Use/Cover Around Thermal Power Plant in Singrauli District, Madhya Pradesh, India," *Spatial Information Research*, vol. 25, pp. 769– 777, 2017. [CrossRef] [Google Scholar] [Publisher Link]
[27] Plant Location Specific Emission Standards. [Online]. Available: https://cea.nic.in/wp-content/uploads/tprm/2020/12/Review_of_Plant_Emission_Standards_29.pdf
[28] USGS Earth Explorer. [Online]. Available: https://earthexplorer.usgs.gov
[29] Xiaolin Zhu, and Eileen H. Helmer, "An Automatic Method for Screening Clouds and Cloud Shadows in Optical Satellite Image Time Series in Cloudy Regions," *Remote Sensing of Environment*, vol. 214, pp. 135–153, 2018. [CrossRef] [Google Scholar] [Publisher Link]
[30] W. Yue et al., "The Relationship Between Land Surface Temperature and NDVI with Remote Sensing: Application to Shanghai Landsat 7 ETM+ Data," *International Journal of Remote Sensing*, vol. 28, no. 15, pp. 3205–3226, 2007. [CrossRef] [Google Scholar] [Publisher Link]
[31] Forough Marzban, Sahar Sodoudi, and Rene Preusker, "The Influence of Land-cover Type on the Relationship between NDVI-LST and LST-$T_{air}$," *International Journal of Remote Sensing*, vol. 39, no. 5, pp. 1377–1398, 2018. [CrossRef] [Google Scholar] [Publisher Link]
[32] IPC–II Division Thermal Power Plants, Environmental Regulations. [Online]. Available: https://cpcb.nic.in/uploads/Thermal_Power_Plant_overview.pdf
[33] L.T. Khemani et al., "Atmospheric Pollutants and Their Influence on Acidification of Rainwater at an Industrial Location on the West Coast of India," *Atmospheric Environment*, vol. 28, no. 19, pp. 3145–3154, 1994. [CrossRef] [Google Scholar] [Publisher Link]
[34] Kyung Hwan Kim et al., "Influence of Wind Direction and Speed on the Transport of Particle-bound PAHs in a Roadway Environment," *Atmospheric Pollution Research*, vol. 6, no. 6, pp. 1024–1034, 2015. [CrossRef] [Google Scholar] [Publisher Link]
[35] Manisha Hariram et al., "Impact of Emissions from Coal-based Thermal Power Plants on Surrounding Vegetation and Air Quality Over Bokaro Thermal Power Plant," *Asian Atmospheric Pollution*, pp. 255– 274, 2022. [CrossRef] [Google Scholar] [Publisher Link]